J. Am. Ceram. Soc., 71 [2] 97-105 (1988)

# Interfacial Layers in Brittle Cracks

DAVID H. ROACH,* SRINIVASARAO LATHABAI,* and BRIAN R. LAWN*

Ceramics Division, National Bureau of Standards, Gaithersburg, Maryland 20899



**A study has been made of interfacial layers that form within cracks in mica and silicate glass. The layers are the result of interactions with environmental species behind the crack tip. Deposition processes are associated with precipitation from aqueous solutions and corrosion of the crack walls. The level of precipitation depends on such factors as "impurity" content, temperature, etc. It is demonstrated that the layers can bridge the interface and thereby significantly increase the apparent toughness and the strength. These retardation effects are modeled as an "internal" (negative) contribution to the net stress intensity factor on the crack from closure tractions over a near-tip area of the interface. The results highlight the potential importance of surface chemistry as a determinant of both equilibrium and kinetic fracture properties.**

## I. Introduction

IT HAS long been established that species in the environment can interact with pristine crack surfaces to augment the driving force for brittle fracture.[1] These interactions may be chemical or physical in nature, and they manifest themselves by modifying the thermodynamic states of the crack system.[2] It would seem that we should expect both equilibrium and kinetic fracture properties to be strongly influenced by the presence of any "corrosion" products at the crack interface.

There has been little attempt in the fracture community to confirm this expectation. One notable study of crack interface corrosion was that of Pulliam,[3] on KCl and NaCl crystals in aqueous solutions and vapors. He observed apparent, steady crack retractions with time, due to precipitation of crystalline material at the narrow interfaces. Pulliam suggested that such crack "healing" should affect mechanical properties. Wiederhorn *et al.*[4] reported the presence of a residual substance in cracks in silicate glass, which they tentatively identified as silica gel, after drying out of capillary condensate. Their results gave no indication that this gel might impede or promote crack growth. Others have proposed specific mechanisms of interaction between corrosion product and crack interface in glasses, e.g., dissolution–reprecipitation ("blunting")[5] and ion-exchange-induced stresses ("alteration layers");[6] the implication in these other studies is that the intrinsic tip configuration must be fundamentally modified. Recently, evidence from strength experiments on glass specimens with controlled (indentation) flaws[7,8] suggests that the source of any such critical modifications of crack structure is to be sought behind, rather than at, the tip, e.g., via an enhanced wall–wall adhesion ("bridging"). Indeed, such a suggestion had been foreshadowed in some earlier Japanese work[9] on the indentation-strength response of chemically treated glass. It is the paucity of experimental data and lack of consensus in theoretical modeling that provide the motivation for the work to be described here.

Accordingly, we present observations of interfacial layers formed within cracks in two archetypal brittle solids, mica and silicate glass, in selected moisture-containing environments. We show that such layers, which may arise from corrosion of the host material or from deposition of environmental impurity species (or both), can extend over substantial distances behind the crack tip, i.e., large enough to retard crack propagation and increase strength by significant amounts. Fracture mechanics modeling in terms of interfacial tractions is used to quantify this retardation. Our results, while not presented as definitive evidence against those mechanisms based on some essential modification of the crack tip structure, do lend support to the bridging concept. We conclude that surface chemistry can be a critical element of the bridging process; however, we make no specific attempt here to elucidate the details of this chemistry, focusing instead on the mechanical implications.

## II. Experiments and Results

In this section we describe observations of crack interface layers in muscovite mica and silicate glasses. These materials were chosen because of their well-controlled fracture behavior and their transparency. Our requirements were for specimens that could be used in conventional crack propagation (double-cantilever beam, double torsion) and strength (indentation flaw) test procedures and that at the same time were amenable to direct viewing of the crack interfaces.

### *(1) Mica*

Our experiments on mica were made using a wedge-loaded cantilever beam arrangement of the kind described originally by Obreimoff[10] and later developed by Bailey.[11] Specimens were cut in plate form with dimensions about 10 mm by 10 mm and 20- to 50-$\mu$m thickness. A blade of thickness 200 $\mu$m was then used to drive a stable cleavage crack partway through each specimen, parallel to the major plate faces (Fig. 1). Control over the wedge position was maintained via a micrometer drive system. The cleavage operation could be observed in situ by mounting the entire wedge-specimen assembly on to the stage of an inverted microscope.[12]

This arrangement proved to be very convenient for both qualitative and quantitative analysis of the crack interface processes. The evolution of corrosion layers under prescribed environmental conditions could be followed readily. Two-beam Fizeau fringes due to interference of light reflected from the opposing crack walls provided a measure of the crack profile. In the thin-beam approximation[13] the profile $y(x)$ behind the tip has (in the absence of any crack-wall tractions) a cusplike inverted parabolic form ($x \ll c$, Fig. 1)

$$2y = 3hx^2/c^2 = m\lambda/2 \tag{1}$$

where $2h$ is the wedge thickness, $c$ is the crack length, $m$ is the fringe order for constructive interference, and $\lambda$ is the light wavelength (mercury light, $\lambda = 0.55$ $\mu$m). Thus by measuring the

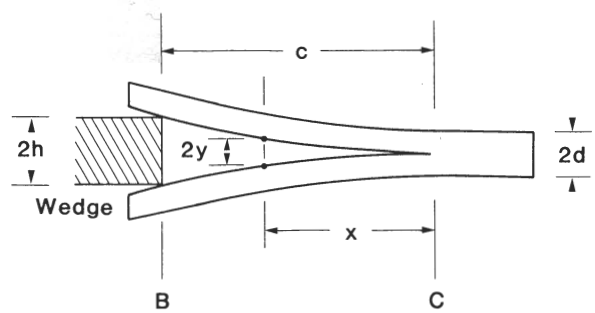


**Fig. 1.** Schematic of wedge-loaded mica DCB specimen.

Manuscript No. 199637. Received March 16, 1987; approved September 17, 1987.
Presented at the 89th Annual Meeting of the American Ceramic Society, Pittsburgh, PA, April 27, 1987 (Basic Science Division, Paper No. 34-B-87).
Supported by the U.S. Office of Naval Research, Metals and Ceramics Program.
*Member, the American Ceramic Society.

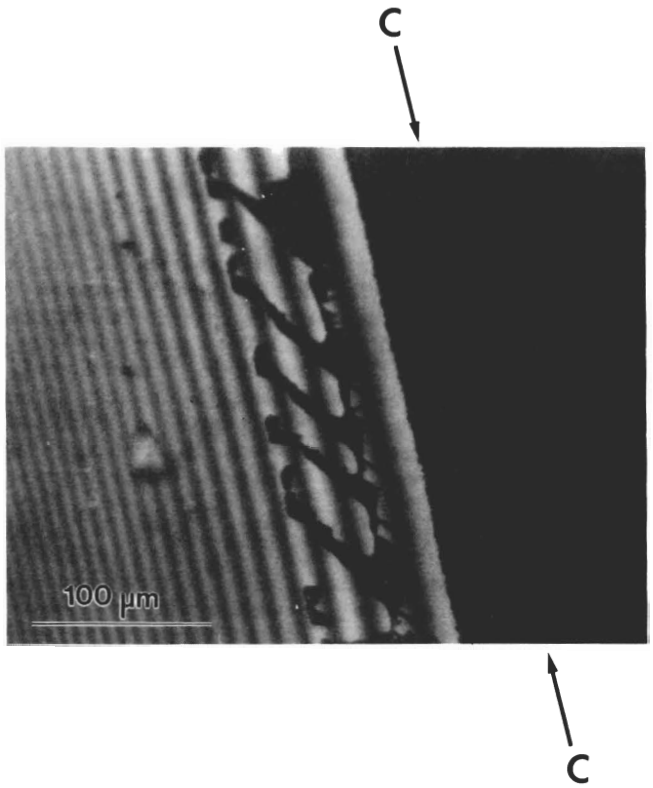


**Fig. 2.** Deposit layers formed in loaded mica DCB specimen on evaporating water from crack interface.

fringe position we could extrapolate back to $m = 0$ to determine the location of the crack tip, and thence to compute the crack driving force.

*(A) Observations of Interfacial Layers:* Let us now look at some examples of layer formation in the mica specimens in selected aqueous environments:

(i) Figure 2 shows an interface formed by first propagating the crack in distilled water and subsequently drying the specimen in a stream of warm air with the wedge still inserted. A deposit is clearly visible behind the tip, in the region between the first and fourth dark fringes (i.e., corresponding to bounds of approximately 0.25- and 1.0-$\mu$m wall separation). Note the dinstict (if not entirely smooth) boundary between the first dark fringe and the extrapolated crack tip (C–C), indicating the presence of another deposit. Of course, the limits of optical resolution preclude us from determining exactly how close to the tip this other layer may extend.

(ii) In Fig. 3 we see a crack initially prepared in a similar way, but later subjected to additional treatment. Thus the deposit between about the 7th and 11th dark fringes was formed as in Fig. 2. The wedge was then advanced into the specimen, causing the crack to propagate unstably several hundred micrometers to the right (see Section II(1*b*)). On fully withdrawing the wedge the crack healed back to about 100 $\mu$m beyond its initial stationary position. The specimen was then aged in laboratory air (25°C, 55% relative humidity (rh)) for 3 months. This aging resulted in the formation of the deposit at right in Fig. 3.

(iii) Figure 4 shows a crack grown in air, then exposed to $10^{-3}M$ KCl solution. KCl was chosen because of the strong healing effects observed in KCl crystals by Pulliam.[3] The solution was admitted to the interface by capillary flow using an eyedropper, then evaporated in warm air, with the wedge fixed. During the drying the meniscus retreated until the entrapped solution became supersaturated, at which point crystallization of the kind described by Pulliam ensued. This crystallization nucleated preferentially at the meniscus and spread rapidly along the interface to produce the observed cubic-symmetry patterns. In more concentrated (e.g., $1M$) solutions the precipitation was so intense as to seal off the near-tip region, dramatically hindering further evaporation of the confined solution.

A closer examination of the KCl precipitation morphology was made by fully fracturing specimens prepared this way and looking at the surfaces in the scanning electron microscope. As we would expect, the region ahead of the original crack tip showed no sign of contamination. However, behind the tip the surfaces were copiously "decorated" with residual deposits. Examples are shown in Fig. 5. In Fig. 5(*a*) we see the cubic crystals characteristic of those formed at the saturation meniscus line (cf. Fig. 4). Closer to the tip, in Fig. 5(*b*), we see much finer, dendritic patterns that were not readily detectable optically. Energy dispersive spectroscopy revealed a strong chlorine peak in both deposition regions of Fig. 5, reinforcing our conviction that the crystallization in this case was indeed forming predominately from the intruding environmental species.

(iv) A similar scanning electron microscope examination was made of cracks exposed to a surfactant solution.* As with the KCl

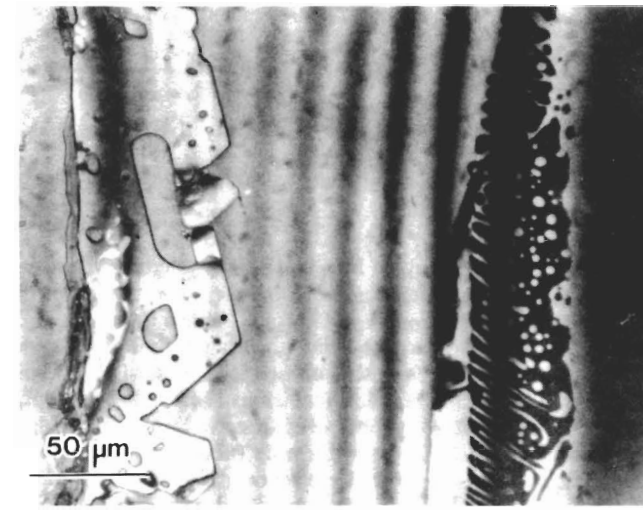


**Fig. 3.** Layers formed as in Fig. 2, but after an additional crack propagation–healing and air-aging treatment with wedge withdrawn.

*Daxad 32 (10 vol% starting concentration), W. R. Grace, Owensboro, KY.

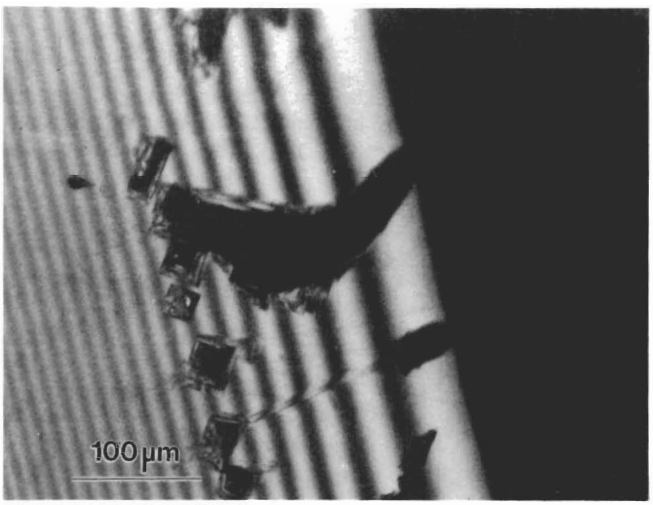


**Fig. 4.** Crystallized layers at crack interface of loaded mica DCB specimen after evaporation of entrapped KCl solution.

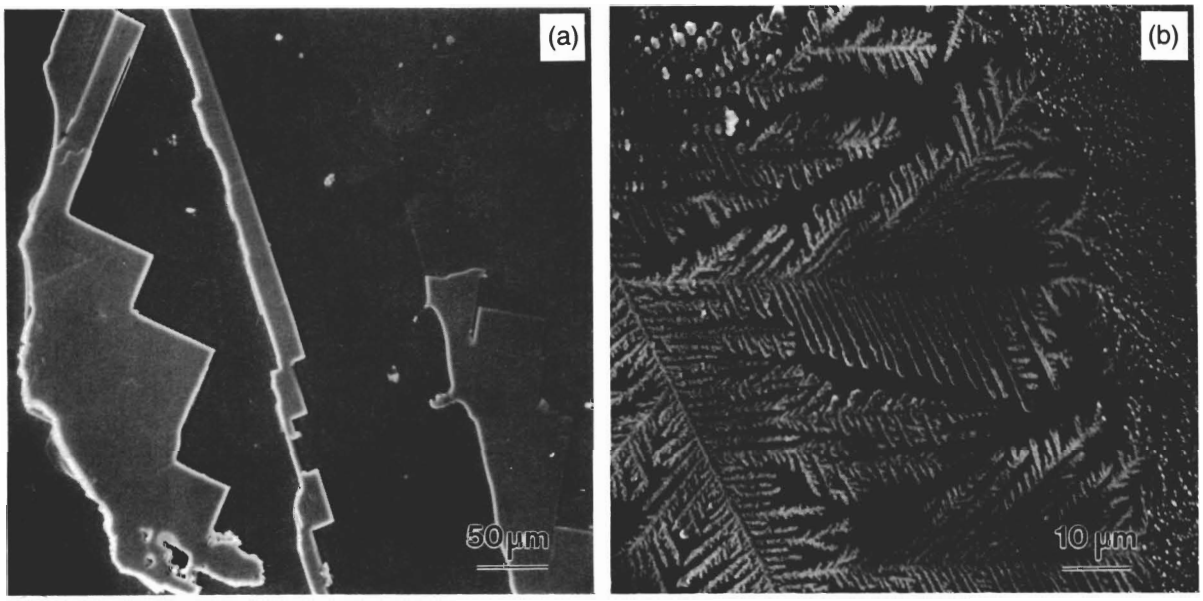


**Fig. 5.** SEM views of fully fractured mica surfaces, showing KCl deposits formed as in Fig. 4: (*a*) region of preferential crystallization at saturated meniscus, (*b*) region of dendritic crystallization closer to the crack tip. Crack propagation direction left to right.

solution we observed striplike layers of residue behind the crack front (Fig. 6). Note, however, the absence of any crystallographic features in this case.

It is therefore clear that interfacial deposits can form in cracks in mica under a variety of environmental conditions. Our observations suggest that liquid environments are the most effective in this regard; however, layers can also develop in air, by capillary condensation. We noted that the morphology was quite reproducible for the high-concentration solutions, but not for the distilled water, implying that in the latter case the precipitation is "impurity sensitive." We also noted that the deposits tended to hold the cracks open as the wedge was withdrawn, but that these same cracks could be induced to retreat again by redissolving the deposits with an injection of fresh water at the interface. Thus there is a strong element of history dependence associated with the interfacial states in mica.

*(B) Effects of Layers on Crack Propagation:* The mica double-cantilever-beam (DCB) geometry is ideally suited to an investigation of the restraining effects of the interfacial layers on subsequent crack propagation. From standard fracture mechanics analysis of this geometry for fixed wedge loading[12,14] we have the "applied" stress intensity factor

$$K_a = 3^{1/2} E h d^{3/2} / 2c^2 \qquad (2)$$

where $E = 170$ GPa is Young's modulus, $2h$ is the wedge thickness, $2d$ is the specimen thickness, and $c$ is the crack length (Fig. 1). Thus by monitoring the crack response as we advance the wedge into the treated specimens we might expect the restraint to be measurable as an excess in $K_a$ over the equilibrium value in the *un*contaminated region.

We have run such tests on specimens of the type described in the previous subsection. The most severe hindrance was noted in the surfactant-treated specimens. A set of micrographs illustrating the observed sequence of events with advancing blade insertion is presented in Fig. 7. The edge of the blade is evident at $B$ in these micrographs. In Fig. 7(*a*) the residual surfactant layer is well delineated behind the crack front $C$. The weak fringe system in this region allows us to locate $C$. With subsequent loading increments in Figs. 7(*b*) and (*c*) we see that while the blade advances, the front remains stationary, corresponding to an increase in $K_a$ in Eq. (2). It is apparent that the interfacial layer is taking up an increasing portion of the applied load. Ultimately, in Fig. 7(*d*), the layer ruptures and the crack jumps unstably to $C'$ until $K_a$ once more attains the equilibrium level for uncontaminated surfaces. It is interesting to note that the original fringe system at $C$ does not disappear as a result of the final propagation stage in Fig. 7(*d*). This suggests that the residual layer must somehow remain intact at the interface. Confirmation is obtained by examining the surfaces along $C$–$C$ after running the crack through the entire specimen, as in Fig. 8. We find completely antisymmetric patterns on opposite halves, indicating that the slivers detach alternately from one wall or the other, but not from both walls simultaneously.

The quantitative results of such tests run in air through surfactant and KCl layers are shown in Fig. 9, as plots of $K_a$ vs blade position (taking the initial stationary position $B$ in Fig. 7(*a*) as reference origin). We note that the resistance associated with the layers can persist for wedge movements of several hundred micrometers. The degree of "toughening" can be substantial, a factor of about 3 for the surfactant. It is clear that the effects that we are dealing with here are far from insignificant.

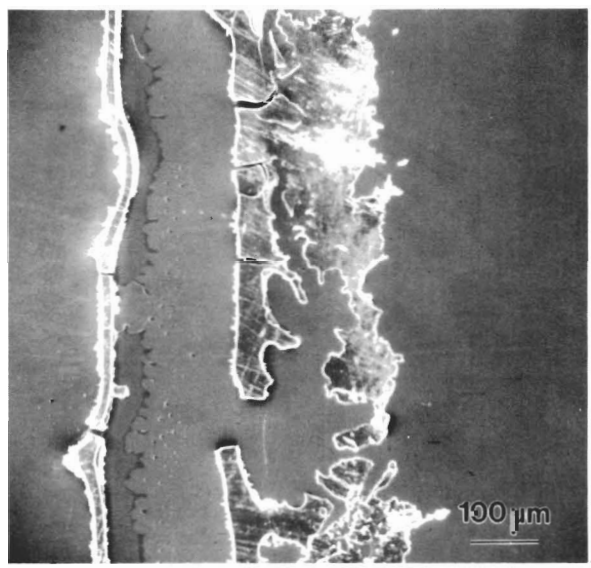


**Fig. 6.** SEM views of mica surfaces formed in surfactant solution. Note lack of crystalline features in residue (cf. Fig. 5). Crack propagation left to right.

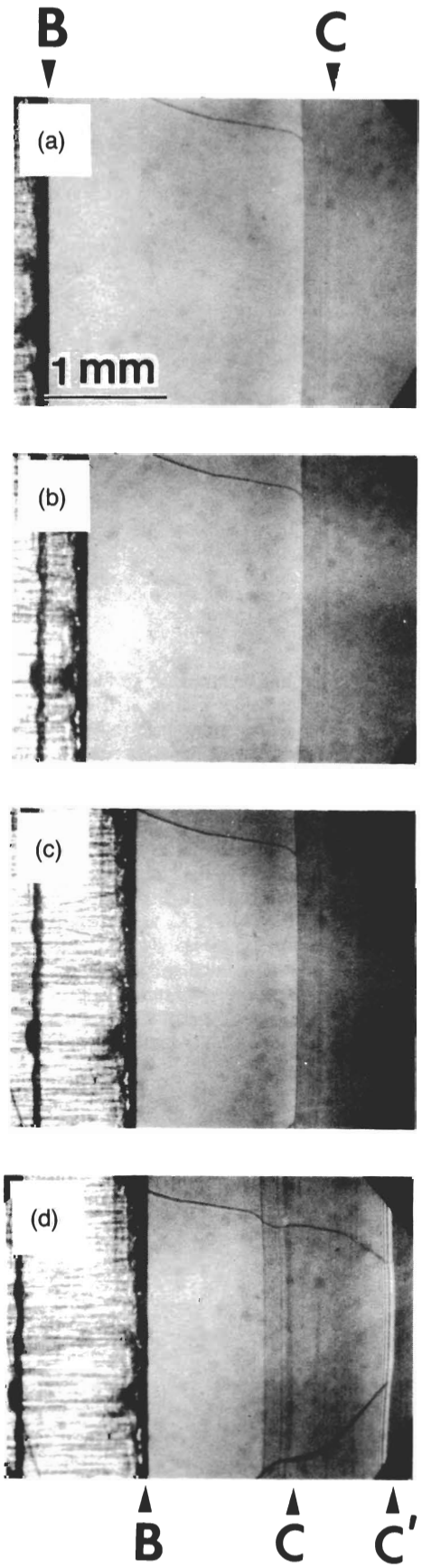


**Fig. 7.** Sequence showing restraining effect of surfactant layer on crack propagation in mica. Layer is observable as weak fringe system to left of *C*. Blade *B* is seen advancing from left in (*a*) to (*c*) until, at (*d*), crack *C* suddenly becomes unstable and propagates to *C'*. (Curved cleavage steps at interface serve as useful crack-plane markers in this sequence.)

*(2) Silicate Glass*

In this part of the study we chose to look at fused silica and soda-lime glasses. For crack propagation conventional beam techniques were used, i.e., DCB and double torsion (DT). Specimens could not be prepared in quite as convenient a configuration for in situ interface observations as in mica, i.e., atomically flat cleavages parallel to thin-sheet faces. The interfaces were nevertheless sufficiently visible in most cases to establish the *presence* of deposits behind the crack tip (the latter located by stress birefringence). The *morphology* of such deposits was determined more readily by examining the glass surfaces after full fracture. For strength analysis indentation cracks were used;[15] these were useful not only for providing a connection between the macroscopic crack observations and "flaw" behavior but also, as we shall see, for allowing us to look more closely at systems in the "loaded" state.

*(A) Observations of Interfacial Layers:* Again, we present selected examples of interfacial layer formation in our glass specimens:

(i) Figure 10 shows the crack surface of a fused-silica DCB specimen which had been aged at 100% rh in air for 6 months.† We see here an optical micrograph of the fully fractured surface; the prolonged exposure to water vapor took place with the crack in an arrested, but loaded, state. The position of the arrested crack front appears to be well delineated (although again it is not possible to determine, within the precision of optical resolution, whether the layer extends completely down to the original front). Note the fingered texture of the layer, indicative of a silica gel.[4,16]

(ii) More extensive layer formation was evident on going to glasses with higher alkali content and raising the temperature during the aging treatment. Thus, Figs. 11 and 12 are micrographs of a soda-lime glass DT specimen before and after full fracture, respectively, in which an air-formed, unloaded crack had been aged for 2 d in distilled water at 80°C. Figure 11 gives an indication that the crack has undergone partial healing during the unloading and that some deposition has occurred during the aging. However, the nature of the interfacial layer is more apparent in the broken specimen (Fig. 12). There we see evidence of enhanced deposition back from the healed crack region where the near-tip interface at the tensile side remained accessible to the aqueous environment during the aging. A similarity may be noted between the interference fringes observed here and earlier in Fig. 8; examination of opposite fracture surfaces, as in the enlargements of Fig. 13, reveals the same characteristic antisymmetry in the patterns.

Qualitative energy dispersive spectroscopy of the surfaces in Figs. 11 to 13 showed little difference between surface compositions ahead and behind the stationary crack front, other than a pronounced magnesium peak in the regions of heavy deposition. This similarity in spectra would suggest that the layer is primarily a corrosion product from the glass walls,[16,17] the magnesium presumably leached out from the bulk glass.

(iii) Figures 14 and 15 are of Vickers indentations in soda-lime glass.[15] In these micrographs we see both radial and lateral crack systems:[18] whereas it is the former which ultimately leads to failure in a strength test[19,20] (see Section II(2*B*)), here the latter provides the clearest views of the interfacial deposits. In Fig. 14 the specimen was indented and then aged in water (*a*) for 6 h at room temperature and (*b*) for a further day at 80°C. Layer formation is apparent in (*b*). Note the persistence of birefringence, indicating that the crack remains partially loaded by residual stresses around the central plastic zone.[7] Figure 15 shows that, given sufficient time (typically, several months), similar layers can form in laboratory air.

Thus in glass, as in mica, we can get substantial layer formation at crack interfaces. Again, the layers are most readily produced in aqueous solutions, but may also result from capillary condensation in air. The process is enhanced by alkali content in the glass and by temperature, consistent with the conventional wisdom concern-

†This figure kindly supplied to us by S. M. Wiederhorn.

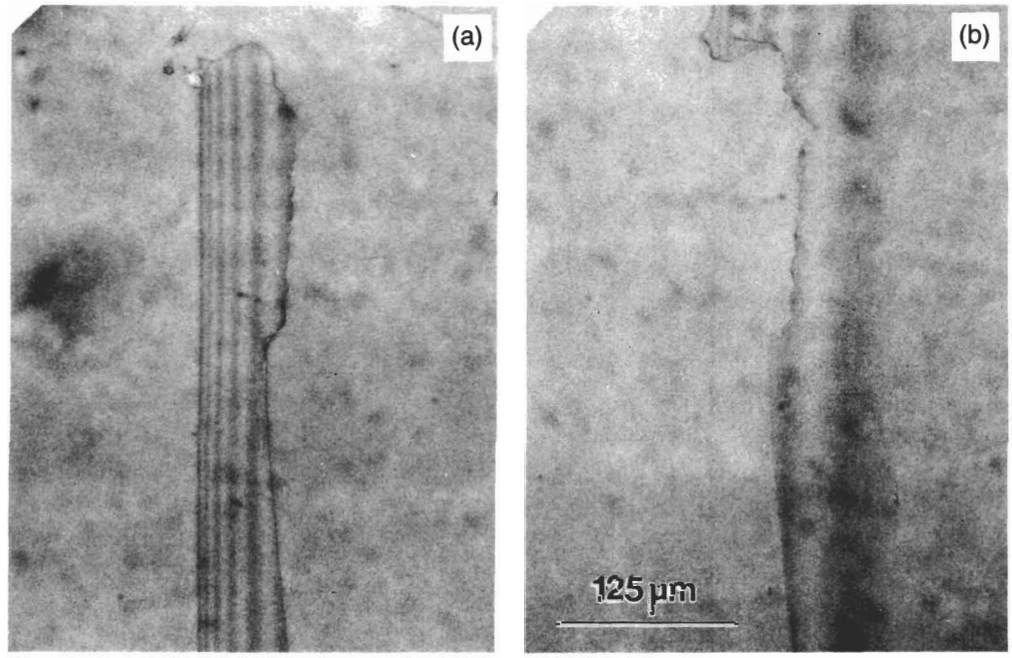


**Fig. 8.** Optical micrographs of "matching" surfaces of specimen in Fig. 7 after full fracture, showing region along crack front $C$–$C$ where detachment of residual layer switches from one face to the other. (Micrograph in (*b*) has been laterally inverted to make "template" effect more apparent.)

ing glass corrosion. It is interesting to reflect that corrosion of the type envisaged here is commonly found in stacks of microscope slides that have been exposed for protracted periods to humid atmospheres; in such instances we have observed adjacent slides to become "cemented" together by the same kind of corrosion product. The strong implication here is that any increased fracture resistance associated with layer formation is attributable to surface–surface and not crack-tip interactions.

*(B) Effect of Layers on Strength:* The Vickers indentation crack system may conveniently be used to examine the potential role of interfacial layers in strength properties. The indentations serve as controlled flaws in flexure specimens.[15,19] A quantitative evaluation of the interfacial tractions can then be made by comparing the strength of specimens *with* layers against controls *without* layers.

We have run such comparative tests on soda-lime glass slides that were exposed to some of the layer-forming environments described above. For the controls, 20-N indentations were aged in water for 1 week at room temperature, to allow the residual stress field to equilibrate and the post-indentation crack growth correspondingly to saturate.[7,8] These specimens were then dried off in a hot air stream for 30 min, covered with a drop of silicone oil, and broken in four-point flexure at high crosshead speed (<50-ms load time to failure) to determine the "inert" strength. Some preliminary

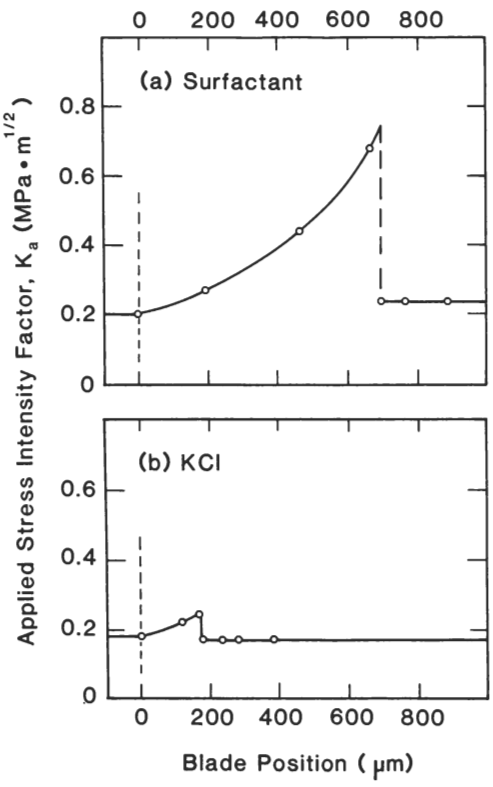


**Fig. 9.** Plot of $K_a$ vs blade position for mica DCB specimens ($d$ = 10 μm) with (*a*) surfactant and (*b*) KCl interfacial layers. Note continuous buildup of resistance until, at rupture point of layer, crack jumps forward to new equilibrium position.

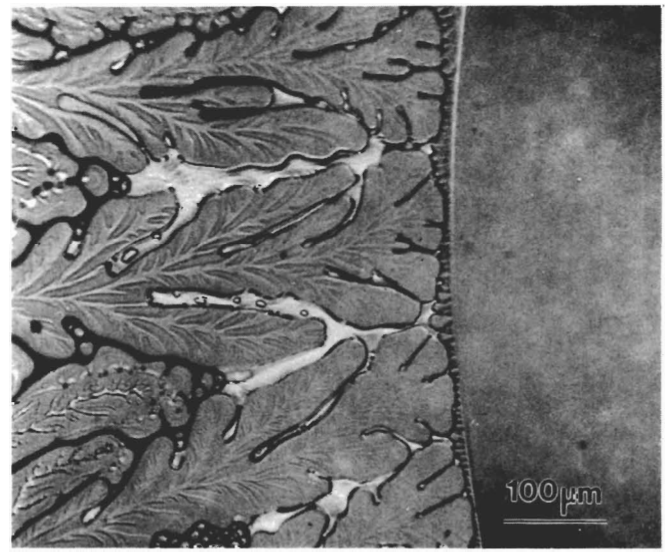


**Fig. 10.** Optical micrograph of fracture surface of fused-silica DCB specimen after exposing the intact interface to saturated water vapor for 6 months. Crack propagation left to right.

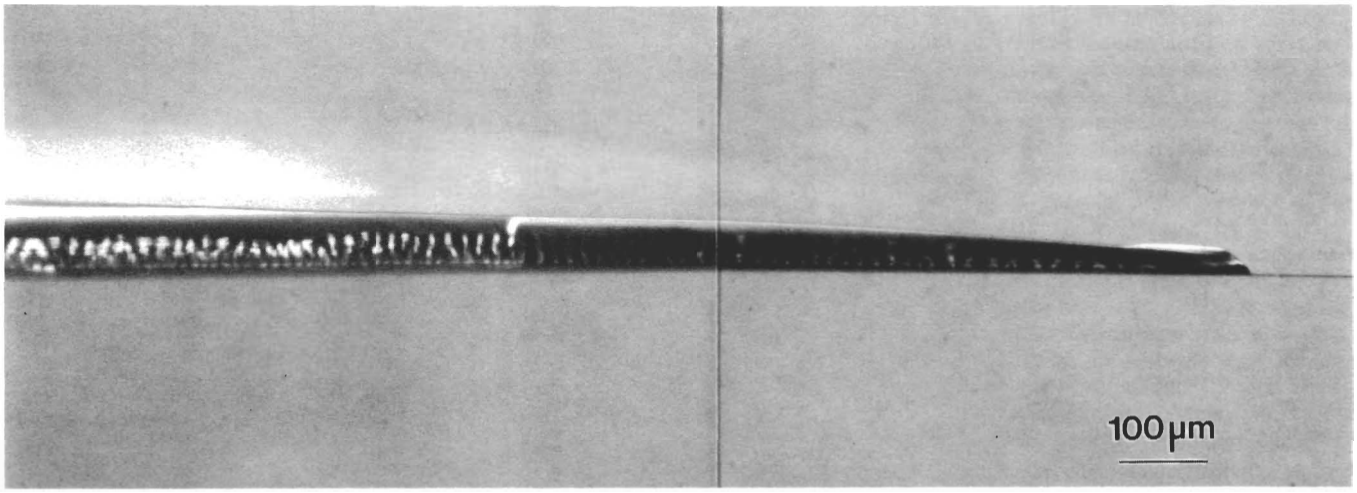


**Fig. 11.** DT specimen of soda-lime glass, viewed in polarized light. Specimen has been unloaded and is slightly tilted to reveal deposits formed as a result of a 2-d exposure to water at 80°C. The faintly visible line ahead of the "apparent" crack front delineates a region of interfacial healing observed during the specimen unloading. (Lower surface is tensile side of specimen.)

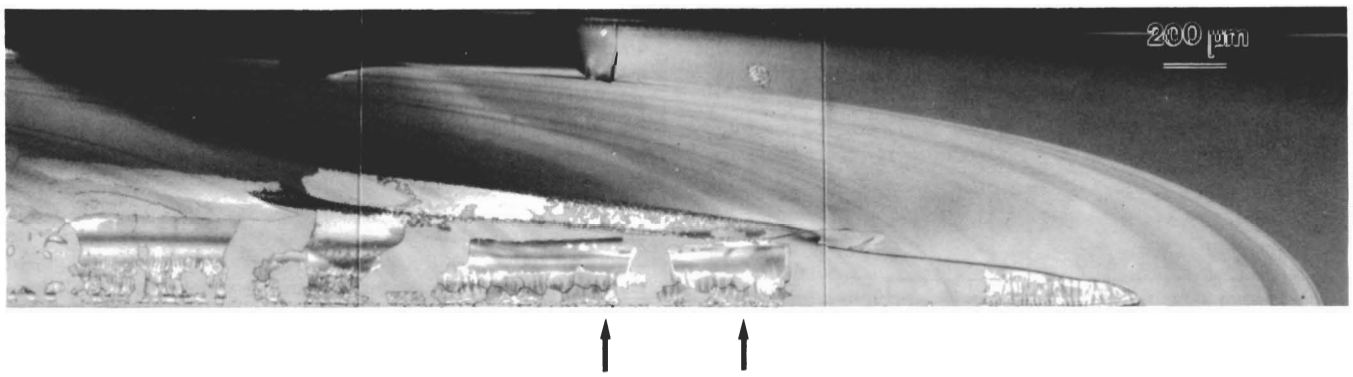


**Fig. 12.** Optical micrograph of broken surface of specimen in Fig. 11. Note absence of residue in healed region. (Arrows indicate region enlarged in Fig. 13.)

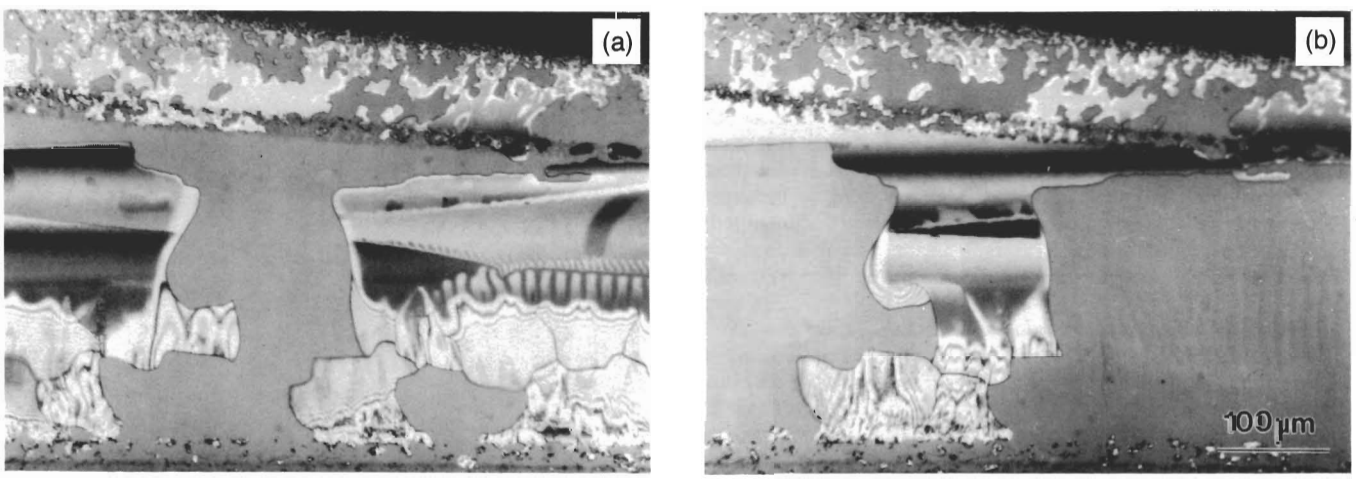


**Fig. 13.** Optical micrographs of same specimen as Figs. 11 and 12, showing matching surfaces. Analogous "template" effect to that in Fig. 8 is observed, indicating alternate detachment of layer from opposing faces. (Micrograph in (*b*) inverted to emphasize template effect.)

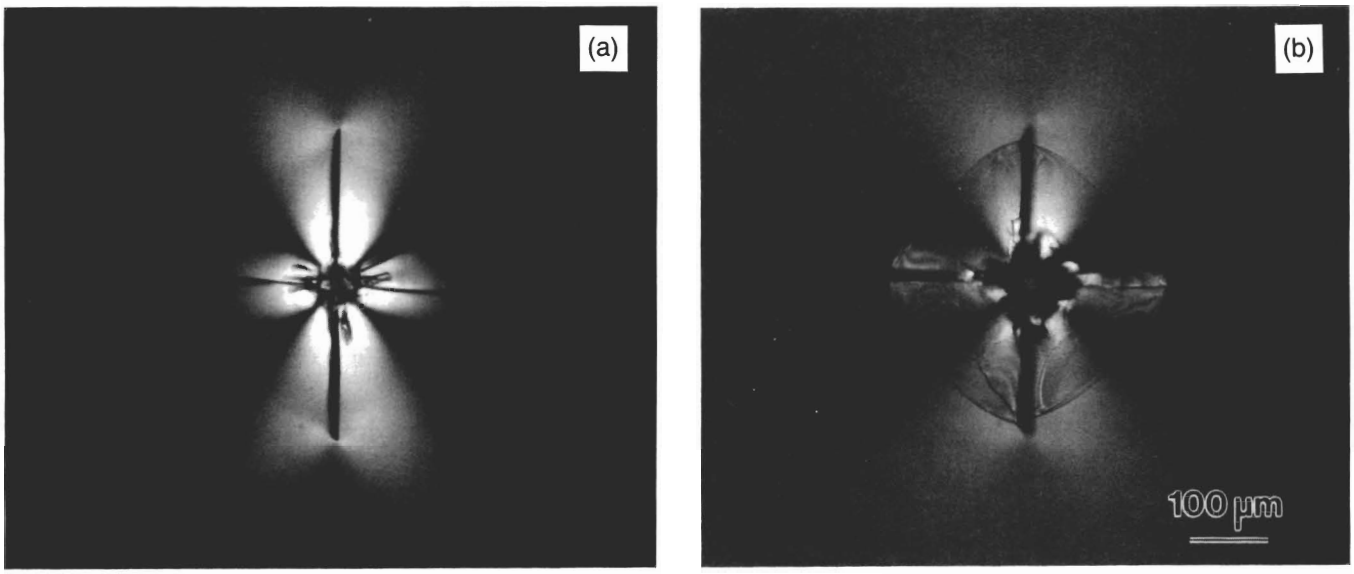


**Fig. 14.** Vickers indentations in soda-lime glass, load 20 N, (*a*) after 6-h aging in water at room temperature (photographed wet), and (*b*) after further 24 h at 80°C (photographed after drying). Layer formation is evident at lateral cracks in (*b*). Viewed in transmitted light with crossed polarizers.

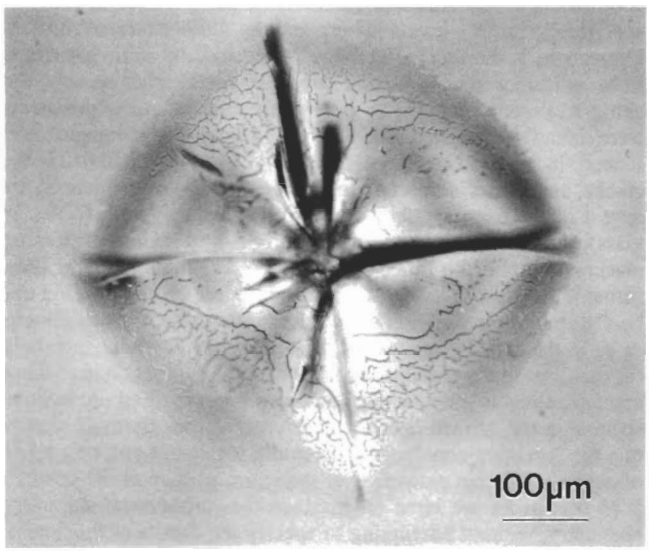


**Fig. 15.** Similar to Fig. 14, but for indentation load of 50 N and aged for 6 months in laboratory air. Viewed in transmitted light.

**Table I. Inert Strengths and Radial Crack Sizes of Soda-Lime Glass Slides with Vickers Indentations (20 N) Subjected to Various Aging Treatments**

| | Strength (MPa) | Crack size (μm) |
|---|---|---|
| Controls | | |
| Aged in water 1 week at 25°C | 81.6 ± 3.8 | 191 ± 5 |
| Same then annealed | 104.6 ± 6.7 | 193 ± 9 |
| Treated specimens | | |
| As for water-aged controls, + extra week in water at 80°C | 146.7 ± 14.5 | 186 ± 3 |
| As for water-aged controls, but surfactant-treated | 129.8 ± 26.0 | 193 ± 3 |

tests were run to confirm that these strengths remain independent of aging time in the saturation region, as found previously,[7] indicating that effects of corrosion are minimal in these specimens. The remaining specimens were given the same initial preparation, but were subjected to an additional aging treatment before breaking. One group was annealed, in air (1 h at 500°C). (This group was actually included as a subset of our controls.) Another group was aged for a second week in water, but after raising the temperature to 80°C. In yet another group the indentations were covered with a drop of concentrated surfactant solution after the initial drying, and then dried out again in warm air. With this last group it was found, as previously,[7] that the inert strengths of specimens remained insensitive to any incremental stable prefailure growths in the radial cracks (induced, for instance, by a small preload cycle

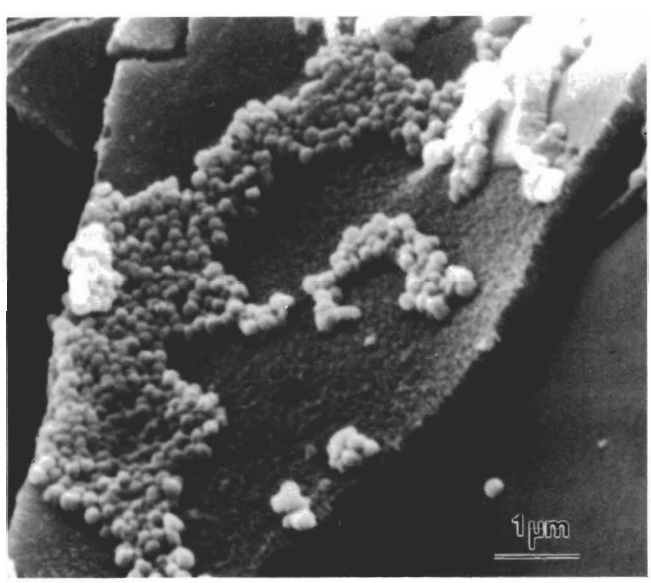


**Fig. 16.** SEM micrograph showing portion of fracture surface of hot-water-aged specimen in Fig. 14(*b*). Severity of corrosion process in this case is apparent.

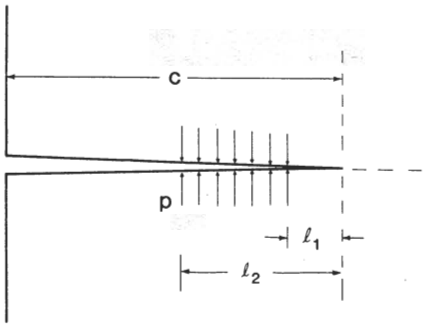


**Fig. 17.** Modeling of layer-induced bridging at crack interfaces. Layer exerts its influence behind tip over strip or annular area for line (DCB, DT) or pennylike (indentation) cracks, respectively.

in air), thereby precluding the possibility that ensuing strengthening effects might be attributable to tip rounding.

The results are summarized in Table I. The strength data are presented as means and standard deviations over an average of 10 specimens per group. (We note that measurements of the radial crack lengths immediately prior to the strength testing, also included in Table I, revealed no detectable differences between any of the groups.) It is clear that we are dealing with significant strengthening effects here; the additional aging in hot water, for instance, has produced a strength increase of almost a factor of 2. Note that such high strengths cannot be attributed to relief of the residual indentation stresses because the annealed control specimens, in which the residual stresses are demonstrably removed altogether,[7] show substantially lower increases (Table I). Examination of the fractured specimens revealed a strong correlation between layer coverage and strength, from apparently contamination-free surfaces (controls) to the totally encrusted surfaces shown in Fig. 16 (hot-water-aged specimens), consistent with a bridging hypothesis.

## III. Discussion

We have presented examples of interfacial layer formation at cracks in mica and glass. We have also demonstrated that these layers can have a measurable effect on mechanical properties, viz., retardation of crack propagation and increase in strength. Our indications are that the interactions can be significant even in seemingly innocuous environments, such as air.

In our interpretation the influence is most properly regarded in terms of restraining tractions at the crack walls behind the tip. (There is a certain analogy here to the interface restraint mechanisms in fiber-reinforced ceramic composites.) The results in Fig. 9 and Table I may therefore be analyzed approximately by modeling the restraint as uniformly distributed closure stresses $p$ between $l_1$ and $l_2$, as in Fig. 17. We consider the two sets of results as follows, leaving detailed calculations to Appendices:

(i) *Mica DCB Specimens (Fig. 1).* In the approximations of $d \ll c$ and $l \ll c$, we can evaluate the closure term as an internal stress intensity factor (Appendix A)

$$K_i = -3^{1/2}p(l_2^2 - l_1^2)/d^{3/2} \tag{3}$$

The absolute value of $K_i$ represents the excess in the measured $K_a$ over the equilibrium level in Fig. 9, e.g., 0.5 MPa·m$^{1/2}$ for the surfactant treatment. Inserting $d = 10$ μm, $l_2 = 150$ μm, and $l_1 = 0$ (lower bound estimate), we obtain $p = 0.4$ MPa.

(ii) *Glass Indentation-Strength Specimens.* Using an analogous analysis for indentation flaws in a uniform applied field, we may compute an appropriate internal stress intensity factor for restraints over the entire penny crack interface ($l_2 = c$, $l_1 = 0$), and thence the inert strength $\sigma$, from the simple superposition relation (Appendix B)

$$\sigma = \sigma_0 + p \tag{4}$$

where the zero subscript denotes control data at a common level of residual indentation stress. For the surfactant-treated specimens in Table I, $\sigma = 129.8$ MPa and $\sigma_0 = 81.6$ MPa (water-aged controls), we obtain $p = 48.2$ MPa. The corresponding internal stress intensity factor is (Appendix B)

$$K_i = -\psi p c^{1/2} \tag{5}$$

Inserting $\psi = 1$ (penny-shaped Vickers flaws[15]) and $c = 180$ μm (Table I) we obtain $K_i = -0.6$ MPa·m$^{1/2}$. An even higher value is obtained for the hot-water-aged specimens.

It is interesting to note that the contribution to the net stress intensity factor from the surfactant treatment is of the same scale in mica and glass. This contribution is a respectable fraction of the intrinsic toughness in both these materials (of order 1 MPa·m$^{1/2}$). On the other hand, the corresponding closure stress $p$ differs markedly in the two cases. It needs to be appreciated that $p$ in our modeling relates to an effective *rupture* stress rather than an intrinsic *cohesive* stress, and the former, as with all extrinsic strength terms, is necessarily sensitive to fracture geometry.

Our modeling of the crack restraint in terms of bridging-type forces warrants futher comment here. We have implied throughout that the effects observed in our mica and glass specimens occur behind, rather than at, the crack tip. The distinction is important because it determines the fundamental source of the bridging forces, viz., *surface* (corrosion) chemistry rather than concerted-reaction *tip* chemistry. Theoretical justification for this conclusion comes from a recent study of the molecular structure of crack interfaces.[21] In that study it is argued that, by virtue of the severe geometrical constraints that characterize the interface at low $K_a$, specifically at $K_a$ levels where cracks slow to zero velocity ("threshold"), the tip is effectively "protected" by steric hindrance from intruding environmental species. We emphasize that the aging treatments that led to layer formation in our experiments were invariably carried out after the cracks had come to rest. Indeed, in our unloaded specimens (e.g., Figs. 3 and 10 to 12) the cracks underwent some healing before aging (as evidenced by retreat of the fringe pattern in mica or of the tip birefringence in glass), thus inevitably rendering the original tip regions even more inaccessible. On the other hand, the contamination layers, once formed, inevitably remain as a persistent force on an unloaded tip, by virtue of their wedging effect on an otherwise retreating interface. In the broader context of fracture behavior *above* threshold (as manifest in the popular accounts of $v$–$K_a$ curves) none of these considerations is intended to play down the role of environmental species in the growth-enhancement process; our thesis is simply that the "reaction zone" is not generally located at one single line of active bonds but extends over the entire surface of the crack.[21]

In this paper we have emphasized the importance of surface chemistry, without attempting to specify the details of this chemistry. A complete description of the fracture process requires these details to be studied. It is conceivable, for instance, that the confined crack interface could act as a chemical "filter," by regulating the concentration of species at the reaction zone (from either the environment or the solid). This notion of a "buffer" zone was first mooted by Wiederhorn,[22] in his interpretation of the $v$–$K_a$ behavior of glasses in acid and base solutions. As a corollary to this reasoning, we may expect diffusion processes to become an increasingly important factor in the crack kinetics in the lower velocity regions.[2] Indeed, as indicated in our mica–KCl experiments (Section II(1*A*)), a particularly heavy deposit might effectively seal off the crack from the environment altogether. In all such phenomena there is an indication of history dependence. Thus, if cracks were to be stopped and later restarted, we should hardly be surprised to observe hysteresis in the $v$–$K_a$ response: this kind of behavior, hitherto interpreted as evidence for blunting,[6] would arise as a natural consequence of any time-dependent buildup of bridging forces in the interfacial reaction zone.

Finally, we may refer briefly to the obvious implications of layer formation on structural considerations. Such formation adds a new element to the fracture mechanics design formalism, and one, moreover, that would appear to confer benefits to the

strength and lifetime properties (counter to the usual deleterious effects of interactive environments). The prospect of improving structural properties by optimizing aging treatments should be motivation enough to gain a deeper understanding of the underlying interfacial chemistry.

## APPENDIX A

### Internal Stress Intensity Factor for DCB Specimens with Interfacial Layers

Consider the contribution to the stress intensity factor for DCB specimens (Fig. 1) from a constant closure stress $p$ in the region $l_2 \leq x \leq l_1$ (Fig. 17). For an incremental line force $F = -p\,dx$ at source point $x$ in this region we have, from beam theory ($d \ll c$),[13] a displacement ($x \ll c$)

$$y(x) = (4F/Ed^3)x^3 \tag{A-1}$$

The corresponding elastic stored energy in the double beam system is simply $2(Fy/2)$

$$U_E = Ed^3y^2/4x^3 \tag{A-2}$$

Then from the Irwin relation for crack driving force, $G = -(\partial U_E/\partial c)_y = K^2/E$,[14] noting from Fig. 1 that $dc = dx$ for fixed line-force position, we compute the internal stress intensity factor associated with the incremental line force $F$

$$dK_i = 12^{1/2}Fx/d^{3/2} \tag{A-3}$$

Integrating over all line forces $F = -p\,dx$ then gives the total layer stress contribution:

$$\begin{aligned} K_i &= -(12^{1/2}/d^{3/2})\int_{l_1}^{l_2} p(x)x\,dx \\ &= -3^{1/2}p(l_2^2 - l_1^2)/d^{3/2} \end{aligned} \tag{A-4}$$

## APPENDIX B

### Internal Stress Intensity Factor and Strength of Vickers-Indented Specimens with Layer Formation

Now consider the corresponding contribution to the stress intensity factor for indentation flaws. We assume, in accordance with our observations in Section II(2*B*), that the "overaged" specimens in Table I are effectively contaminated over the entire area of exposed crack interface; i.e., the closure stress $p$ acts over the full radial distance between $l_1 = 0$ (origin of half-penny crack configuration) and $l_2 = c$ (crack radius). Then the stress intensity factor has the familiar form for uniform fields

$$K_i = -\psi pc^{1/2} \tag{B-1}$$

where $\psi$ is a dimensionless geometrical quantity.

If such an indentation flaw is used in a strength test, the *net* stress intensity factor is

$$\begin{aligned} K &= K_a + K_i + K_r \\ &= \psi\sigma_a c^{1/2} - \psi pc^{1/2} + \chi P/c^{3/2} \end{aligned} \tag{B-2}$$

The $K_a$ term is due to the uniform applied stress $\sigma_a$; the $K_r$ term is due to the residual field associated with the contact deformation zone, characterized at indentation load $P$ by the dimensionless quantity $\chi$.[15,19,20] The condition for equilibrium is $K = K_c$, where $K_c$ is the "toughness": this equilibrium condition is sufficient for failure, *provided* the additional, instability requirement $dK/dc > 0$ is met.[23] It has been demonstrated elsewhere[7] that such a proviso *is* met for "fully aged" specimens of the type described in Table I (effectively, for specimens in which relaxation processes have reduced $\chi$ to the point where the $K_r$ term no longer exerts a significant stabilizing influence on the crack system[20]). Under these conditions we can solve Eq. (B–2) in a straightforward manner to determine the strengths $\sigma_a = \sigma$ for $p > 0$ (with layers) and $\sigma_a = \sigma_0$ for $p = 0$ (without layers, i.e., controls). The solutions are particularly simple where $K_r$ is unchanged (fixed $P, c, \chi$) between treated and control specimens: we obtain the simple superposition relation

$$\sigma = \sigma_0 + p \tag{B-3}$$

**Acknowledgments:** The authors thank S. M. Wiederhorn for providing the initial stimulation for this work. His observations of residual gel layers in DCB specimens from earlier studies, of which Fig. 10 is one example, led us to look for layer formation at mica interfaces.

## References

[1] S. M. Wiederhorn, "Influence of Water Vapor on Crack Propagation in Soda-Lime Glass," *J. Am. Ceram. Soc.*, **50** [8] 407–14 (1967).
[2] B. R. Lawn and T. R. Wilshaw, Fracture of Brittle Solids; Ch. 7 and 8. Cambridge University Press, London, 1975.
[3] G. R. Pulliam, "Precipitation in Microscopic Cracks," *J. Am. Ceram. Soc.*, **42** [10] 477–82 (1959).
[4] S. M. Wiederhorn, A. G. Evans, and D. E. Roberts; pp. 829–41 in Fracture Mechanics of Ceramics, Vol. 2. Edited by R. C. Bradt, D. P. H. Hasselman, and F. F. Lange. Plenum, New York, 1974.
[5] S. Ito and M. Tomozawa, "Crack Blunting of High-Silica Glass," *J. Am. Ceram. Soc.*, **65** [8] 368–71 (1982).
[6] B. C. Bunker and T. A. Michalske; pp. 391–411 in Fracture Mechanics of Ceramics, Vol. 8. Edited by R. C. Bradt, A. G. Evans, D. P. H. Hasselman, and F. F. Lange. Plenum, New York, 1986.
[7] B. R. Lawn, K. Jakus, and A. C. Gonzalez, "Sharp vs Blunt Hypotheses in the Strength of Glass," *J. Am. Ceram. Soc.*, **68** [1] 25–34 (1985).
[8] D. H. Roach and A. R. Cooper, "Effect of Contact Residual Stress Relaxation on Fracture Strength of Indented Soda-Lime Glass," *J. Am. Ceram. Soc.*, **68** [11] 632–36 (1985).
[9] N. Shinkai and S. Furuuchi, "Effect of Silane Coupling Agents in Artificial Crack on the Strength of Glass," *Rep. Res. Lab., Asahi Glass Co., Ltd.*, **25** [1] 1–11 (1975).
[10] J. W. Obreimoff, "The Splitting Strength of Mica," *Proc. R. Soc. London, A*, **127** [805] 290–97 (1930).
[11] A. I. Bailey, "Friction and Adhesion of Clean and Contaminated Mica Surfaces," *J. Appl. Phys.*, **32** [8] 1407–12 (1961).
[12] D. H. Roach, D. M. Heuckeroth, and B. R. Lawn, "Crack Velocity Thresholds and Healing in Mica," *J. Colloid Interface Sci.*, **114** [1] 293–94 (1986).
[13] R. J. Roark, Formulas for Stress and Strain, 4th ed.; Ch. 8. McGraw-Hill, New York, 1965.
[14] B. R. Lawn and T. R. Wilshaw, Fracture of Brittle Solids; Ch. 3. Cambridge University Press, London, 1975.
[15] D. B. Marshall and B. R. Lawn; pp. 26–46 in Microindentation Techniques in Materials Science and Engineering, ASTM STP 899. Edited by P. J. Blau and B. R. Lawn. American Society for Testing and Materials, Philadelphia, PA, 1986.
[16] R. K. Iler, The Colloidal Chemistry of Silica and Silicates. Cornell University Press, Ithaca, 1955.
[17] L. L. Hench and D. E. Clark, "Physical Chemistry of Glass Surfaces," *J. Non-Cryst. Solids*, **28** [1] 83–105 (1978).
[18] B. R. Lawn and T. R. Wilshaw, "Indentation Fracture: Principles and Applications," *J. Mater. Sci.*, **10** [6] 1049–81 (1975).
[19] D. B. Marshall and B. R. Lawn, "Residual Stress Effects in Sharp Contact Cracking: I" *J. Mater. Sci.*, **14** [8] 2001–12 (1979).
[20] D. B. Marshall, B. R. Lawn, and P. Chantikul, "Residual Stress Effects in Sharp Contact Cracking: II," *J. Mater. Sci.*, **14** [9] 2225–35 (1979).
[21] B. R. Lawn, D. H. Roach, and R. M. Thomson, "Thresholds and Reversibility in Brittle Cracks: An Atomistic Surface Force Model"; unpublished work.
[22] S. M. Wiederhorn, "A Chemical Interpretation of Static Fatigue," *J. Am. Ceram. Soc.*, **55** [2] 81–85 (1972).
[23] Y.-W. Mai and B. R. Lawn, "Crack Stability and Toughness Characteristics in Brittle Solids," *Annu. Rev. Mater. Sci.*, **16**, 415–39 (1986). □